Electronic Supplementary Information

Fouling is the beginning: Upcycling biopolymer-fouled substrates for fabricating high-permeance thin-film composite polyamide membranes

Ruobin Dai, [a] Hongyi Han, [a] Tianlin Wang, [a] Jiayi Li, [a] Chuyang Y. Tang, [b] and Zhiwei Wang *[a]

[a] State Key Laboratory of Pollution Control and Resource Reuse, Shanghai Institute of Pollution Control and Ecological Security, School of Environmental Science and Engineering, Tongji University, Shanghai 200092, China

[b] Department of Civil Engineering, the University of Hong Kong, Pokfulam Road, Hong Kong S.A.R., China

To whom all correspondence should be addressed.

Tel.: +86-21-65975669, Fax: +86-21-65980400, E-mail address: zwwang@tongji.edu.cn

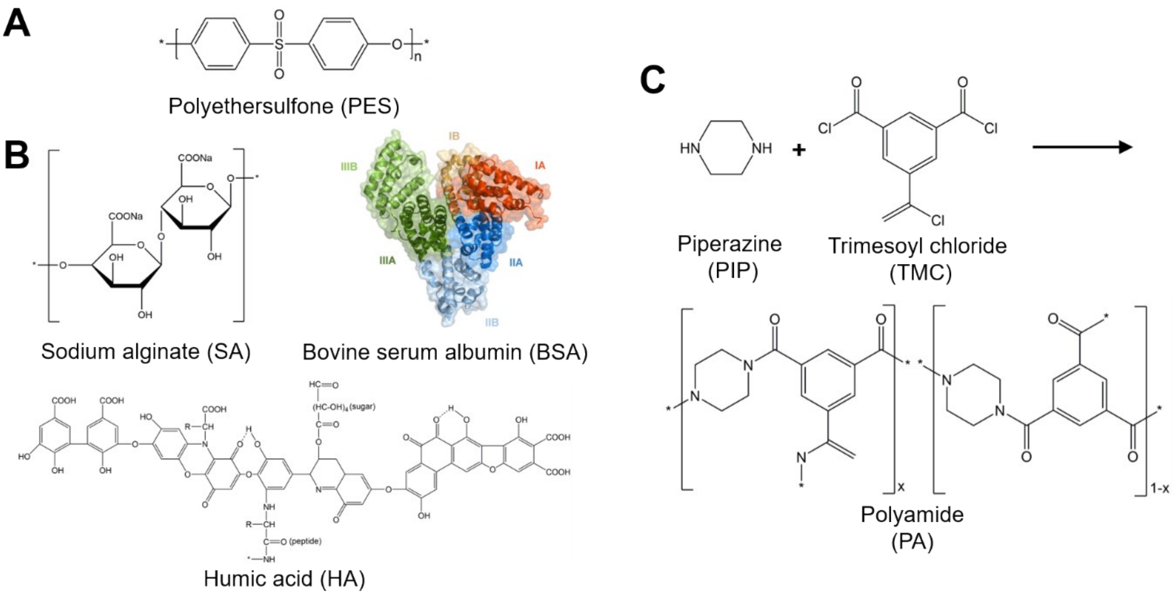

Figure S1. Details of the materials and chemicals used. (A) Structure of PES membrane as substrate; (B) Structure of sodium alginate, bovine serum albumin (adapted with permission from Majorek et al.[1]) and humic acid (adapted from Melo et al.[2] and Stevenson et al.[3]); (C) Structure of the two monomers used for polymerization reaction

Extraction and characterization of microbial EPS

Microbial EPS was thermally extracted from activated sludge collected from the Bailonggang Municipal Wastewater Treatment Plant, Shanghai, China. The extraction procedure was according to the literature.[23] Fifty milliliters of well-mixed sludge were washed with 0.9% NaCl twice after centrifugation at 8000 rpm for 10 min at 4 °C. The collected cells were resuspended in 0.9% NaCl followed by thermal extraction at 60 °C for 1 h. The mixture solution was centrifuged at 10000 rpm for 15 min at 4 °C and the supernatant was freeze-dried for further use. Note that the extracted EPS did not contain microorganisms, and therefore further membrane fouling by EPS only belonged to organic fouling rather than biofouling. The contents of carbohydrates, humic substances and proteins were determined by the Anthrone method and the modified Lowry method according to the literature.[37] The polysaccharides, proteins and humic substances in EPS were 176 mg, 269 mg and 540 mg per gram of EPS, respectively. The molecular size distribution of extracted EPS was determined by Gel Permeation Chromatography (GPC), LC-20AD, Shimadzu.

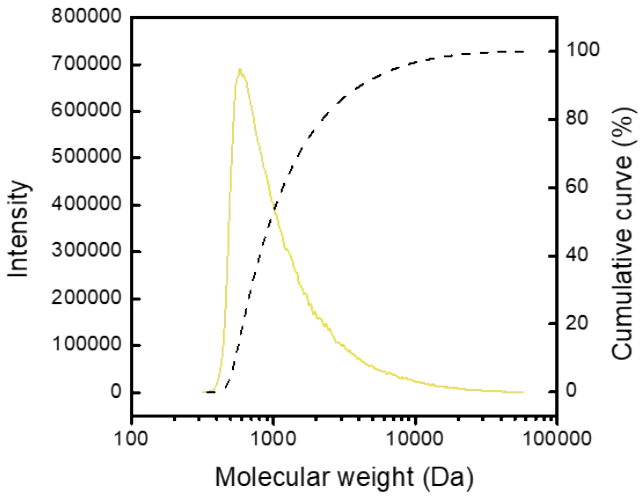

Figure S2. Molecular size distribution of extracted microbial extracellular polymeric substances.

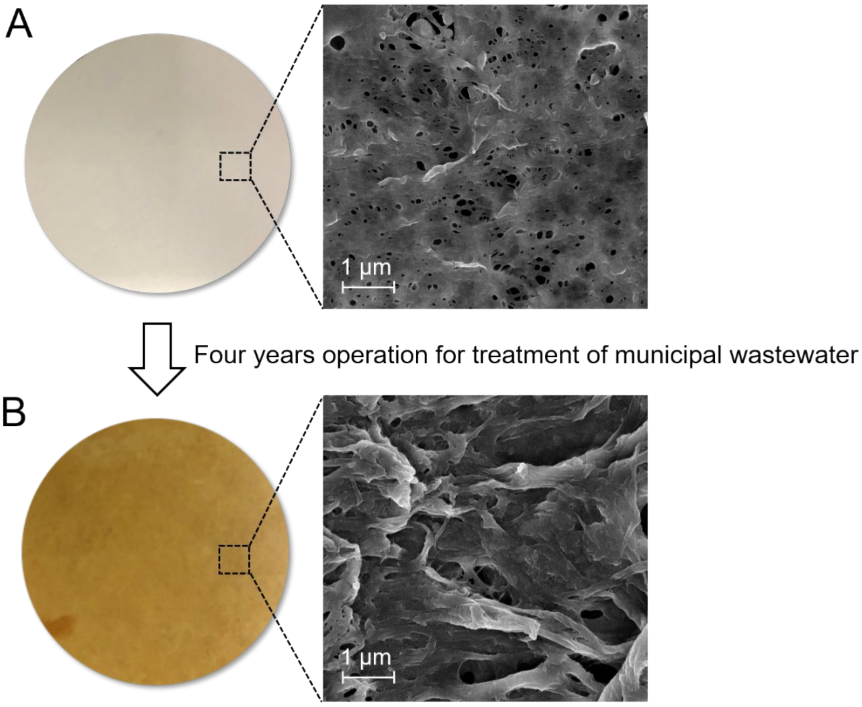

Figure S3. Photo and SEM characterizations of unfouled (A) and fouled (B) TP7 MF membrane. Photo credit: Ruobin Dai.

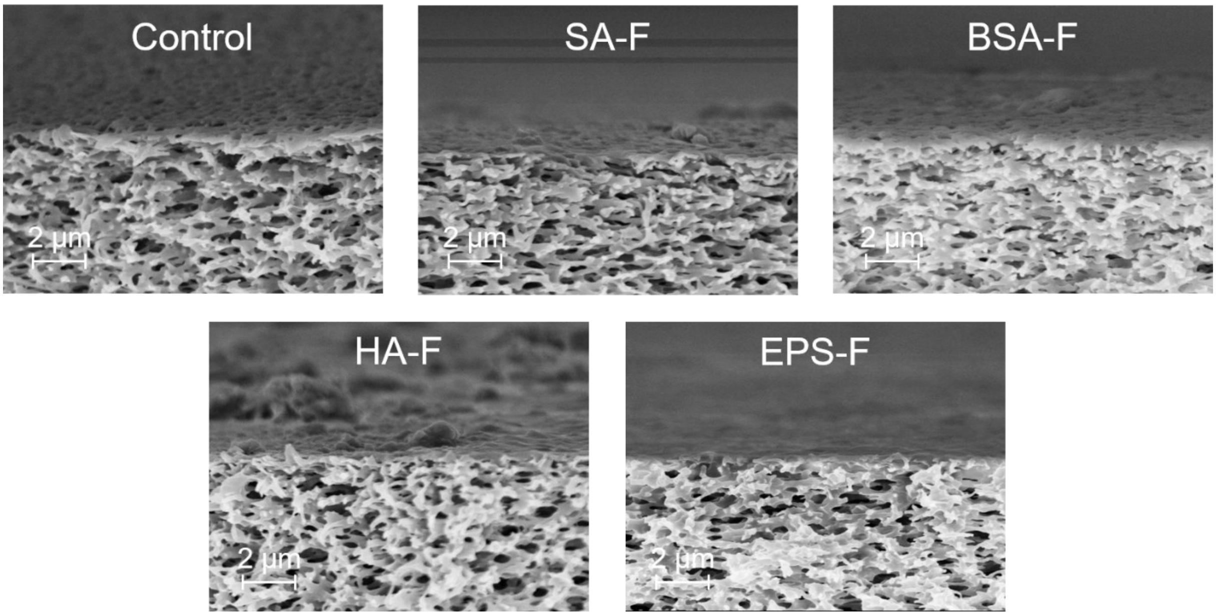

Figure S4. Cross-section SEM characterizations of different biopolymer fouled substrates.

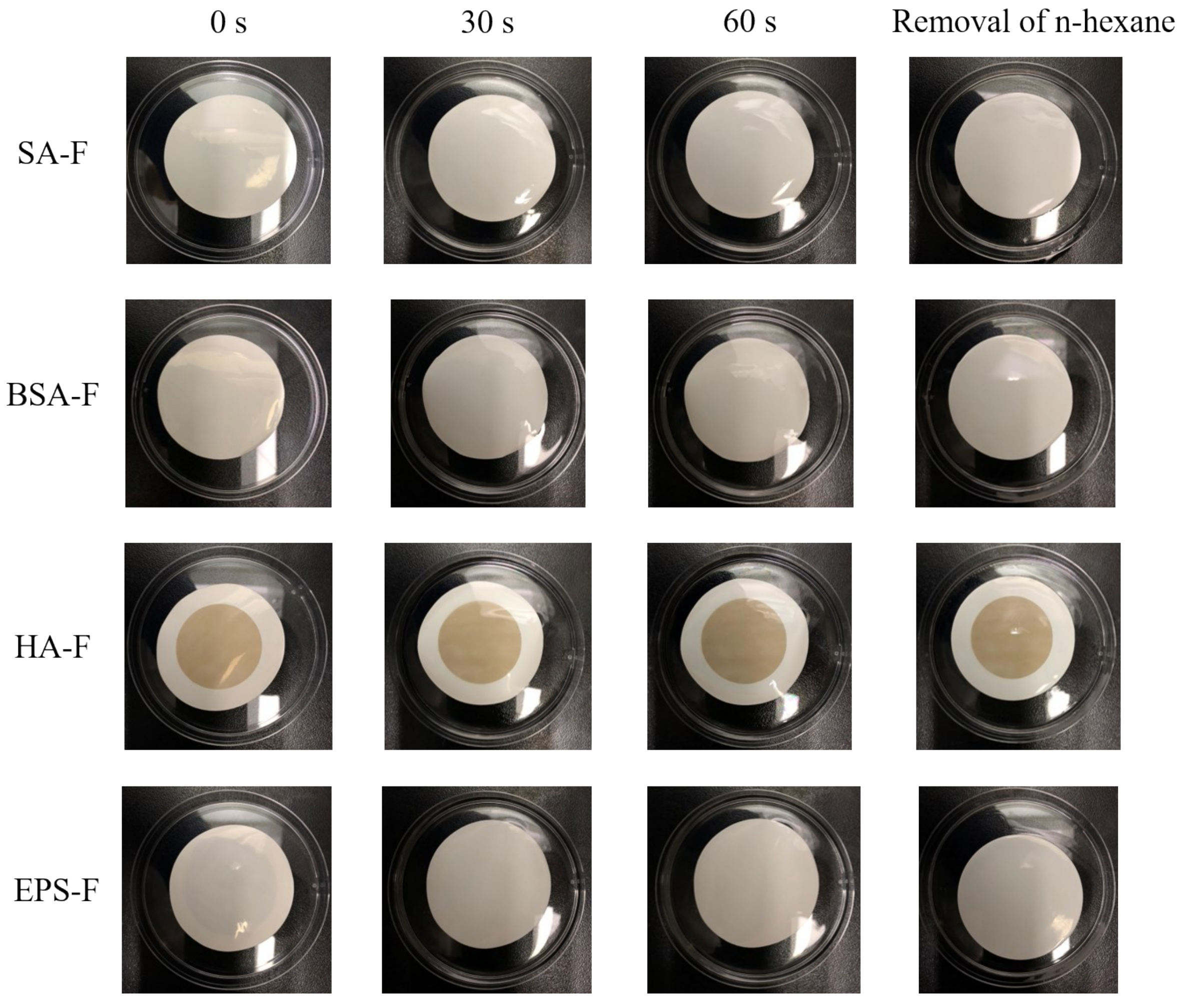

Figure S5. PES MF substrate fouled by various biopolymers showing excellent stability in the short-term exposure to *n*-hexane.

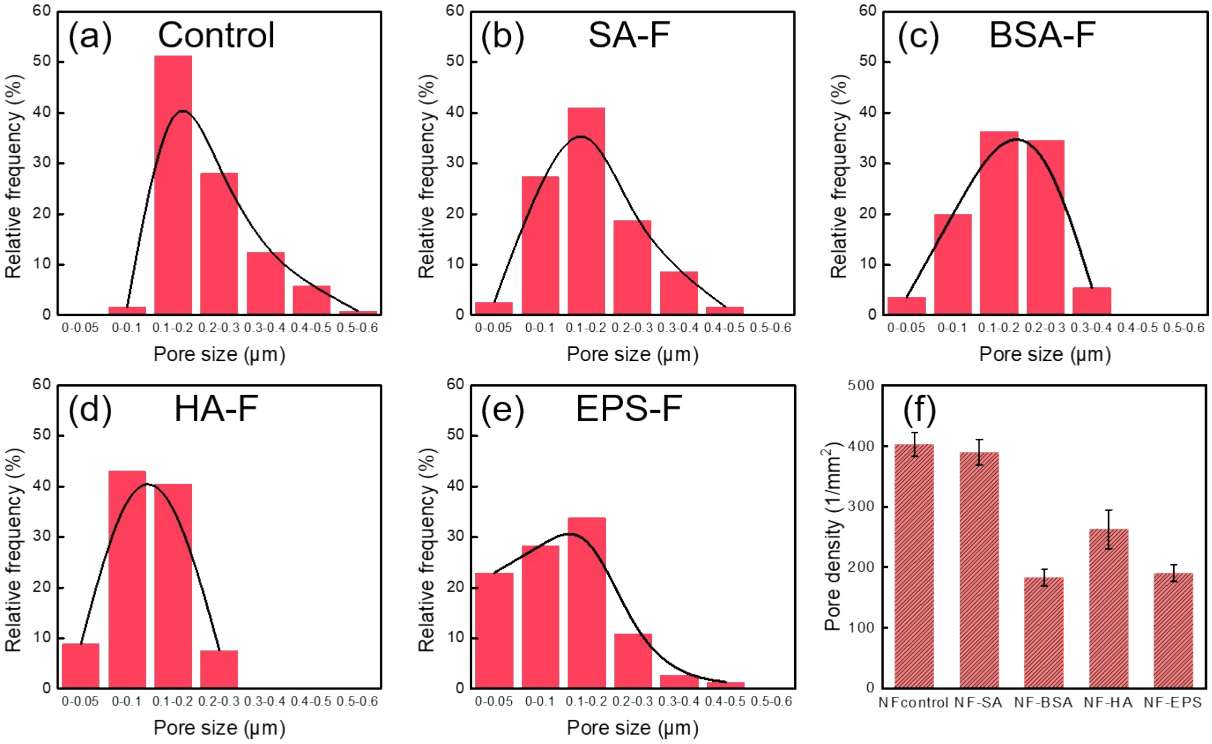

Figure S6. Pore size distribution (a-e) and pore density (f) of clean and biopolymer fouled PES microfiltration substrates.

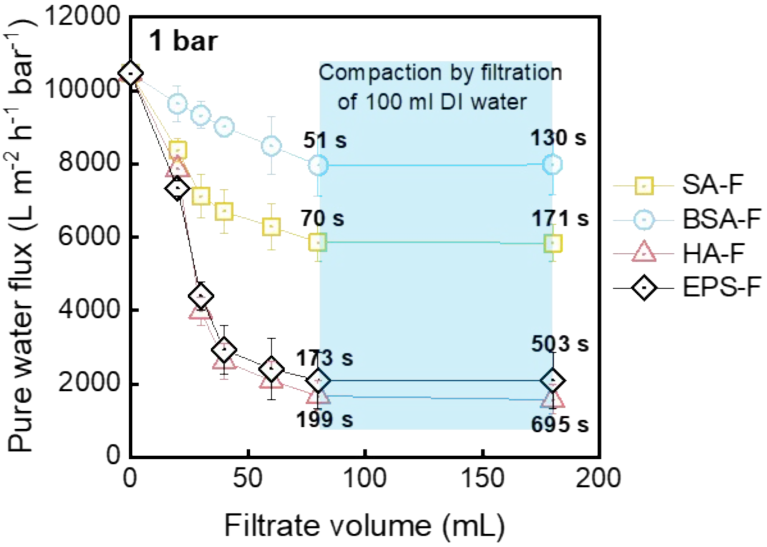

Figure S7. Flux decline profiles of PES microfiltration substrates fouled by various biopolymer foulants. The flux decline profiles of PES substrates by different biopolymer foulants presented different tendencies. The PWF of fouled PES substrates declined to ~20% to ~80% of the initial flux, which is comparable to those of the typical fouled/end-of-life flux[6]. Note that 0.9 bar pressure was applied throughout the fouling and compaction experiments on the microfiltration substrates.

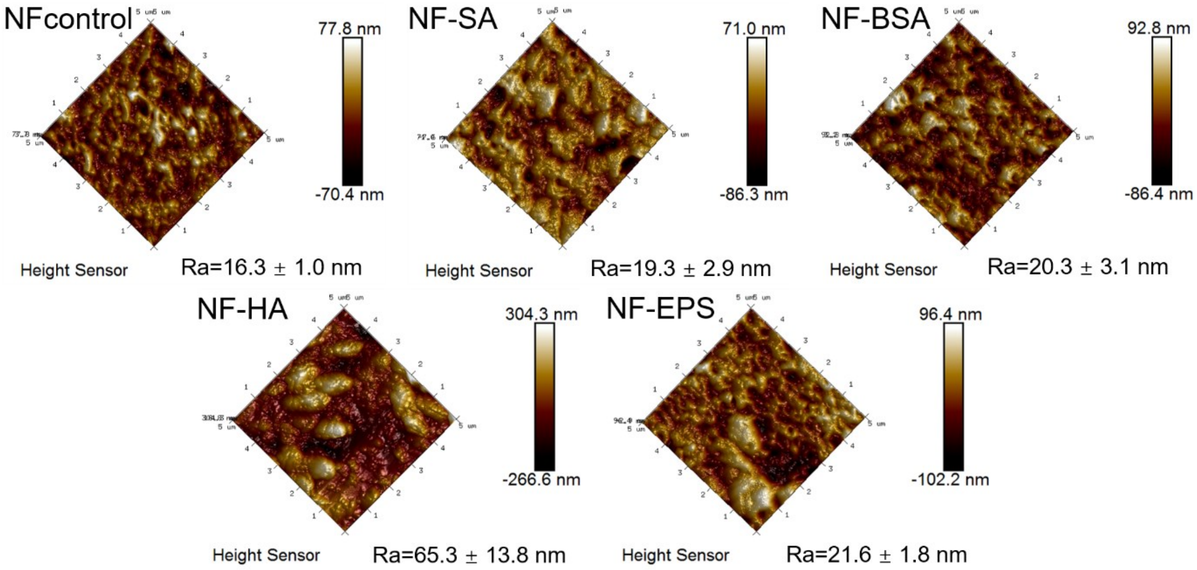

Figure S8. Surface roughness of clean and biopolymer-fouled PES microfiltration substrates.

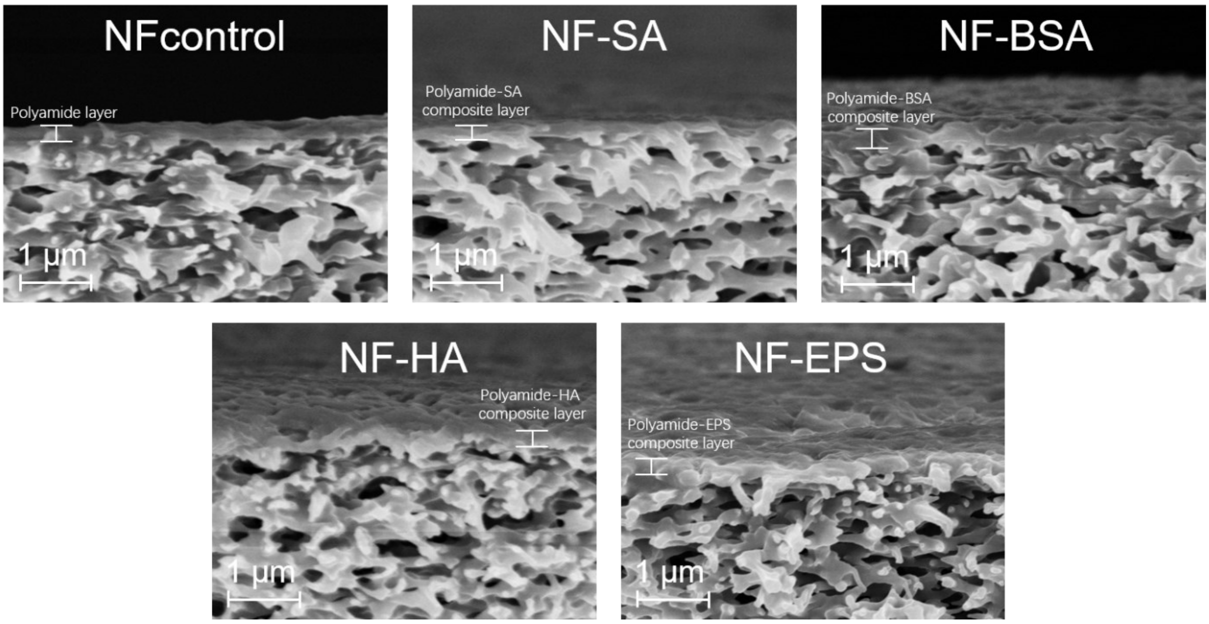

Figure S9. Cross-section SEM characterizations of polyamide TFC membranes based on different substrates.

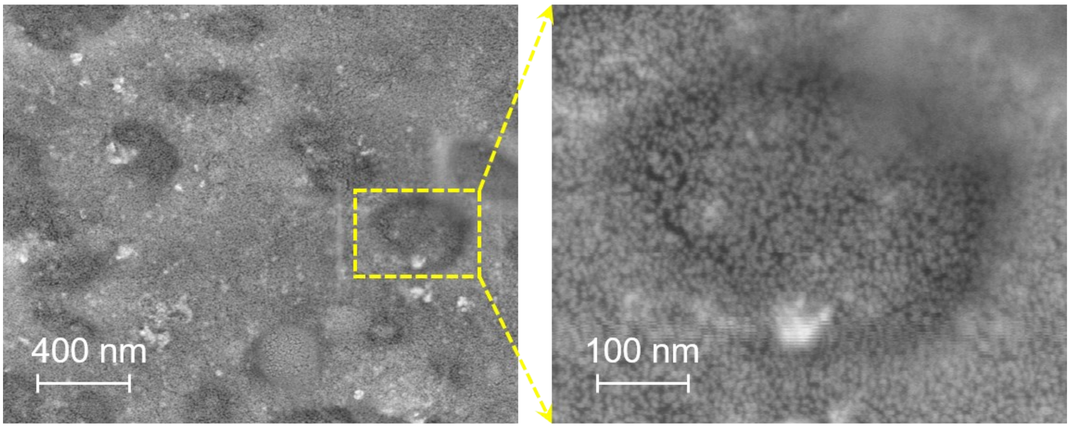

Figure S10. Magnified SEM images focused on the pore-like structure on NF-EPS membrane

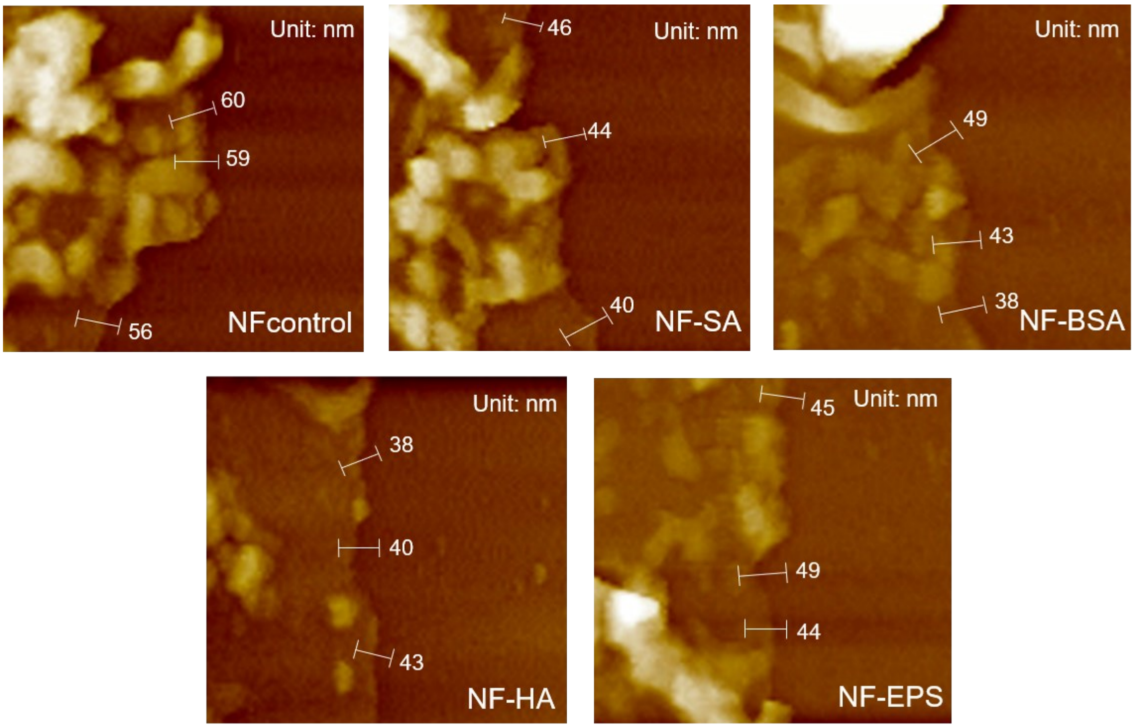

Figure S11. AFM scan reveals thickness of polyamide layer of TFC membranes.

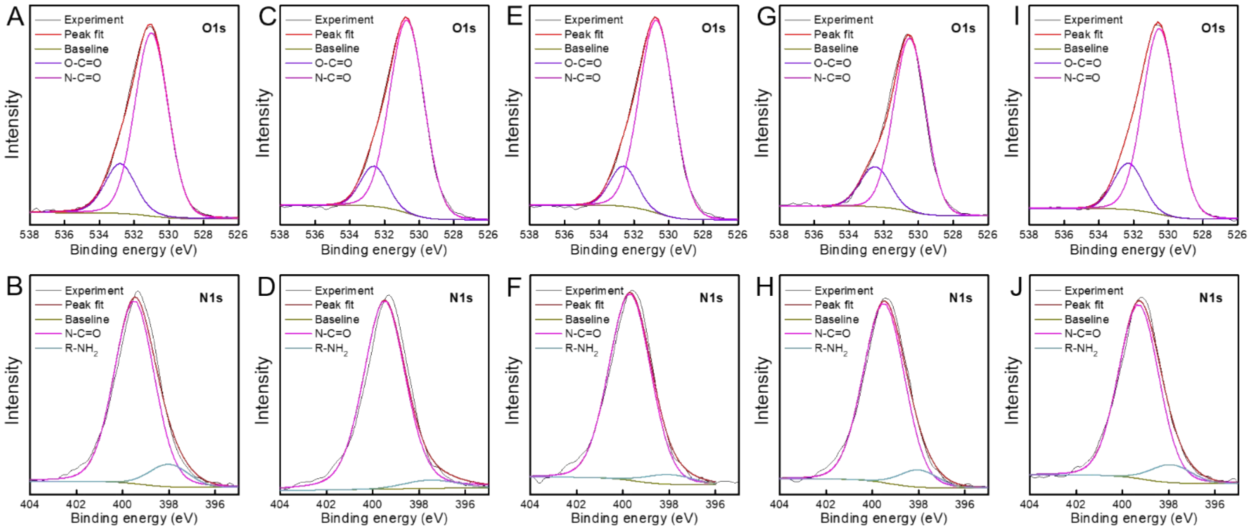

Figure S12. Narrow scan results of X-ray photoelectron spectra of polyamide TFC membranes. (A, B) NFcontrol; (C, D) NF-SA membrane; (E, F) NF-BSA membrane; (G, H) NF-HA membrane; (I, J) NF-EPS membrane.

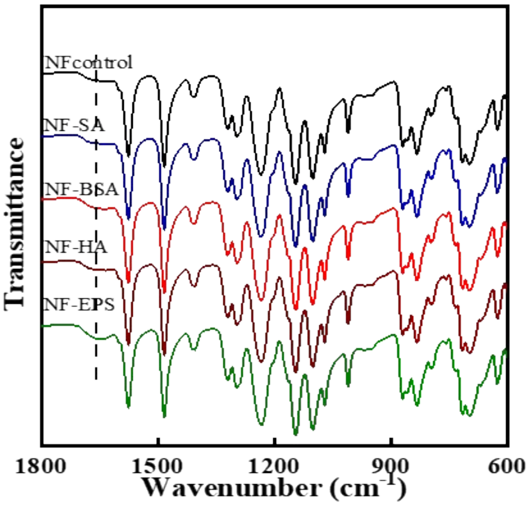

Figure S13. ATR-FTIR characterization of various upcycled PA membranes

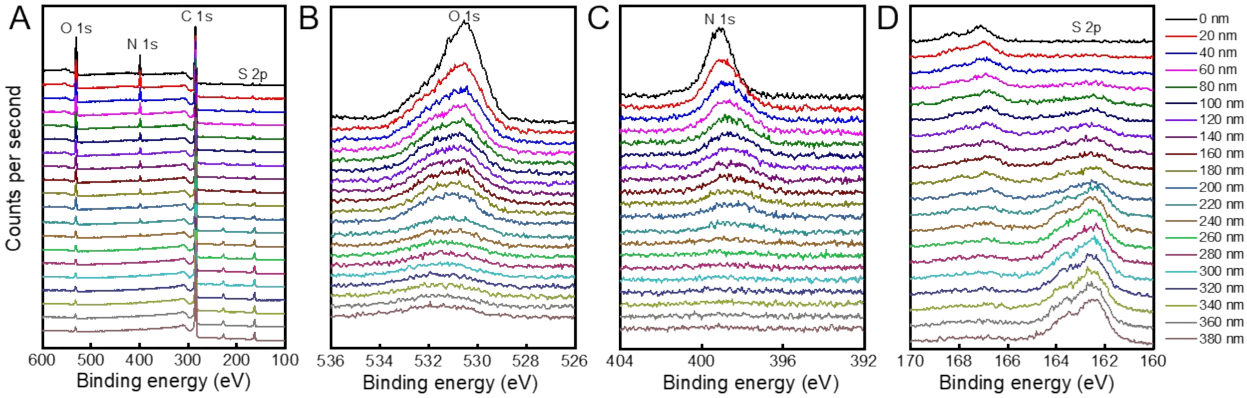

Figure S14. XPS depth profiles of the NF-SA membrane: (A) Survey spectra; (B) high-resolution spectra of oxygen (O 1s orbital); (C) high-resolution spectra of nitrogen (N 1s orbital); (D) high-resolution spectra of sulfur (S 2p orbital). The etching rate was 20 nm/s and the spectra were acquired after each second of etching.

XPS Ar^+ ion-beam sputtering was used for obtaining depth profiles of the NF-SA membrane. The sputtering time was set to 40 s and the spectra were acquired with 5 s waiting time after each sputtering. Both survey and high-resolution spectra were acquired over a spot on the membrane surface of approximately 400 μm in diameter with ~100 W beam power. For depth profiling, Ar^+ ion beam with ion energy 3000 eV was used in the Monatomic mode to raster over an area of 2 mm in diameter on the membrane surface. For the survey spectra, the pass energy is 150 eV over the testing range of 0−1350 eV with 1 eV resolution and 100 ms dwell time. The survey data were then averaged over 10 scans. High-resolution XPS spectra of S 2p and N 1s were acquired with 0.06 eV resolution and 25 eV pass energy with 200 ms dwell time, and averaged over 10 scans. The spectra were corrected using C 1s at 284.8 eV as the internal reference.

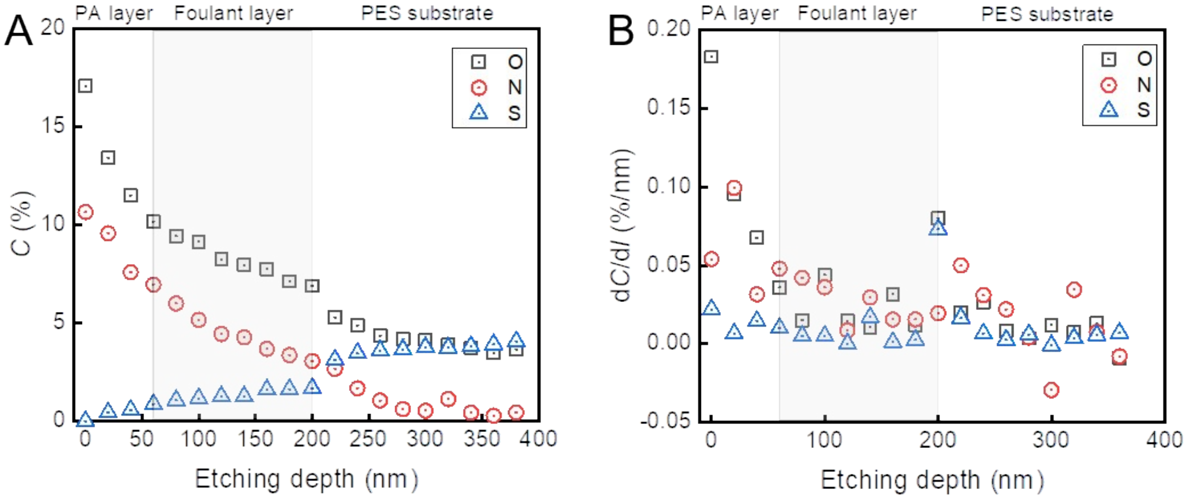

Figure S15. (A) XPS depth profile of different elements for the NF-SA membrane, *C* represents the atomic percentage of each element; (B) Absolute values of d*C*/d*l*, where *l* represents etching depth for each sputtering cycle, 20 nm. By analyzing both data from *C* and d*C*/d*l*, the XPS depth profile can be divided into three zones that represent PA layer, foulant layer, and PES substrate as shown in figures.

The results showed that the O 1s and N 1s peaks quickly decreased during the Ar^+ ion beam sputtering from 0 nm to 60 nm, indicative of the etching through PA layer. The d*C*/d*l* of O 1s and S 2p significantly changed at etching depth of 200 nm, suggesting that the ion beam had already reached the skin of PES substrate.

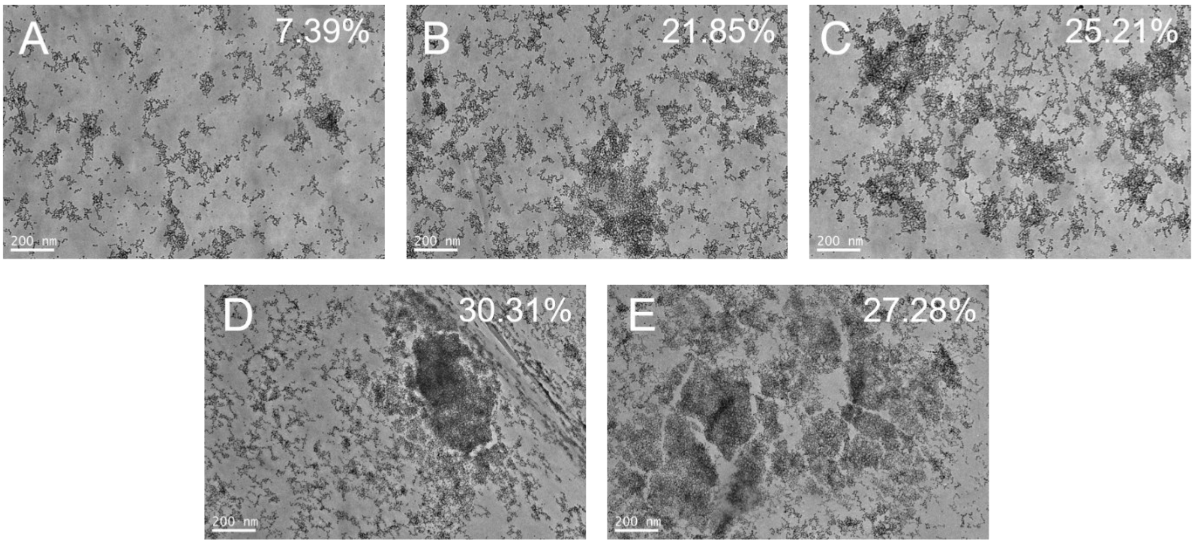

Figure S16. Projected area TEM micrographs of the pristine and biopolymer-based TFC PA membranes filtrated with 5 nm gold nanoparticle. (A) NFcontrol; (B) NF-SA; (C) NF-BSA; (D) NF-HA; (E) NF-EPS membranes. The value in the right corner of each images correspond to the percent area coverage for the image. The deposition of GNPs on the surfaces of the biopolymer-fouled membranes was significantly different (more uniform, $p<0.05$) from that on the NFcontrol. These results all highlight that the foulants between the PA layer and substrate can create additional channels for water transport.

Preparation of TFC PA membranes on EPS spray-coated substrate

The prepared EPS solution (10 mg/L) was spray coated on the PES microfiltration substrate using an airbrush (FUJ-819918, Fujiwara) at 0.1 bar and at a 20 cm distance from the membrane at room temperature. The deposition amount of EPS on the surface was equal to that on/inside the EPS-fouled PES substrate. After drying at 40 °C for 1 h, the EPS-coated PES substrate was subjected to IP between PIP in water (0.05 wt/v %) and TMC in *n*-hexane (0.04 wt/v %).

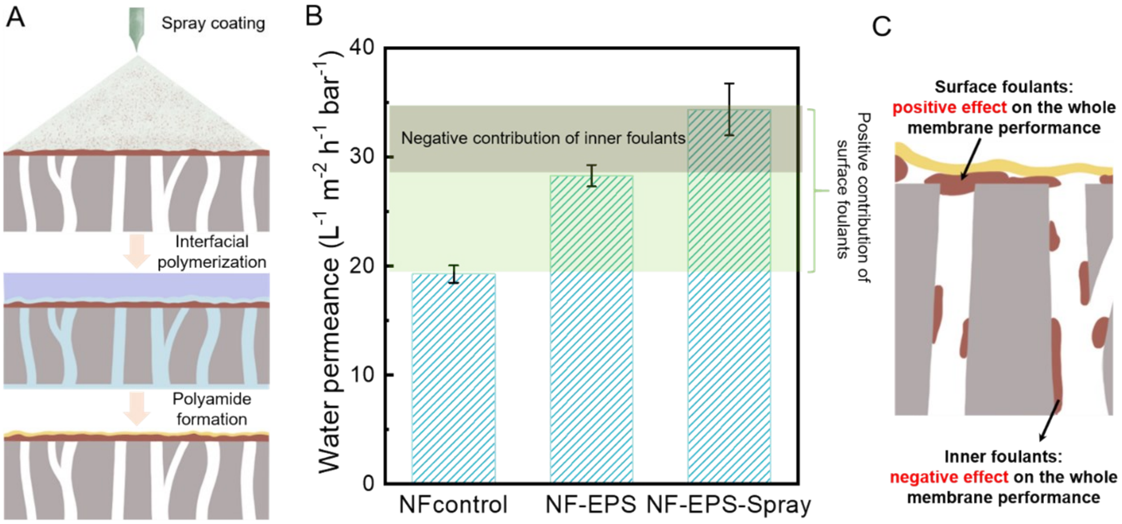

Figure S17. Contribution of surface and inner foulants to the whole membrane transport property of the upcycled NF-EPS membrane. (A) Schematic illustrating the fabrication of the TFC PA membrane on a biopolymer spray-coated substrate; (B) Contribution of surface and inner foulants to the water permeance of the NF-EPS membrane; (C) Schematic of the contribution of surface and inner foulants to the whole membrane performance.

The IP reaction was further applied on the substrate spray-coated by EPS to form a PA active layer (Figure S17A). After exclusion of the effect of inner foulants, we noticed that the water permeance of NF-EPS was enhanced from 28.3 to 34.4 L m^{-2} h^{-1} bar^{-1} without losing Na_2SO_4

rejection (Figure S17B). Therefore, we can infer that the surface foulants have a positive effect on the whole NF-EPS membrane performance in terms of changes in the surface properties, increases in PIP uptake and mediation of the water transport pathway, while the inner foulants cause a negative effect due to the increase in resistance of the whole membrane to water (Figure S17C). Understanding the roles of foulants at different positions on/inside the substrates is beneficial for fabricating TFC PA membranes with higher performance based on fouled MF/UF membranes in the future.

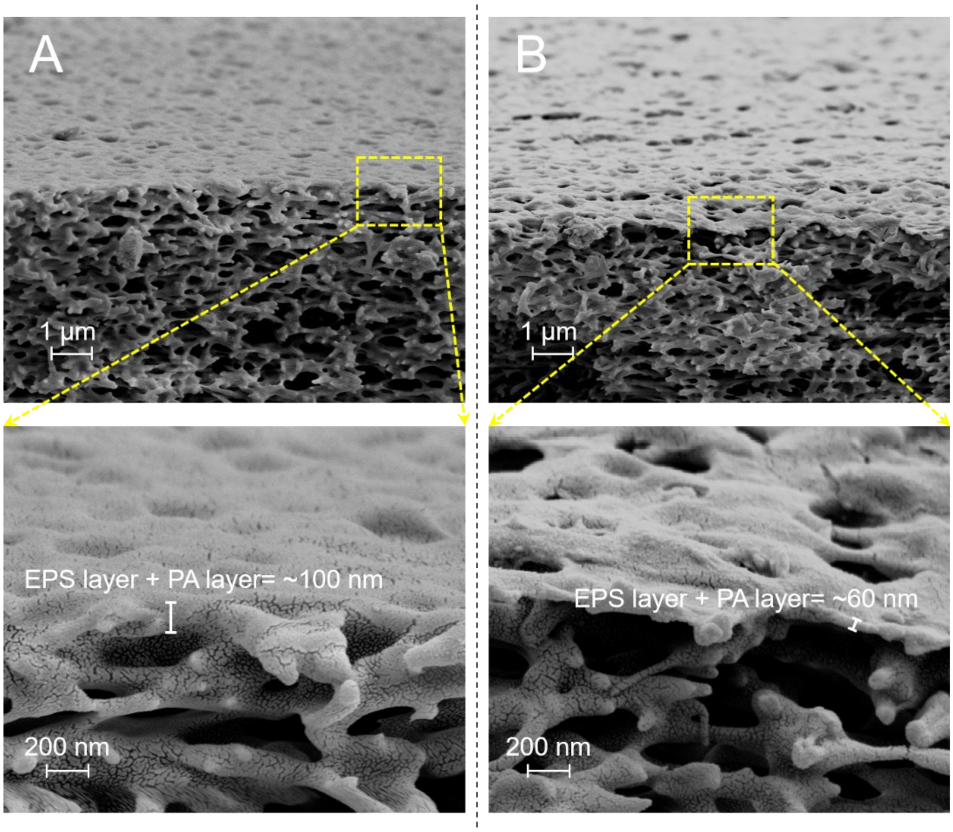

Figure S18. Compaction phenomenon of PA layer and EPS foulant layer by 16 bar pressure for 4 h: (A) before compaction; (B) after compaction.

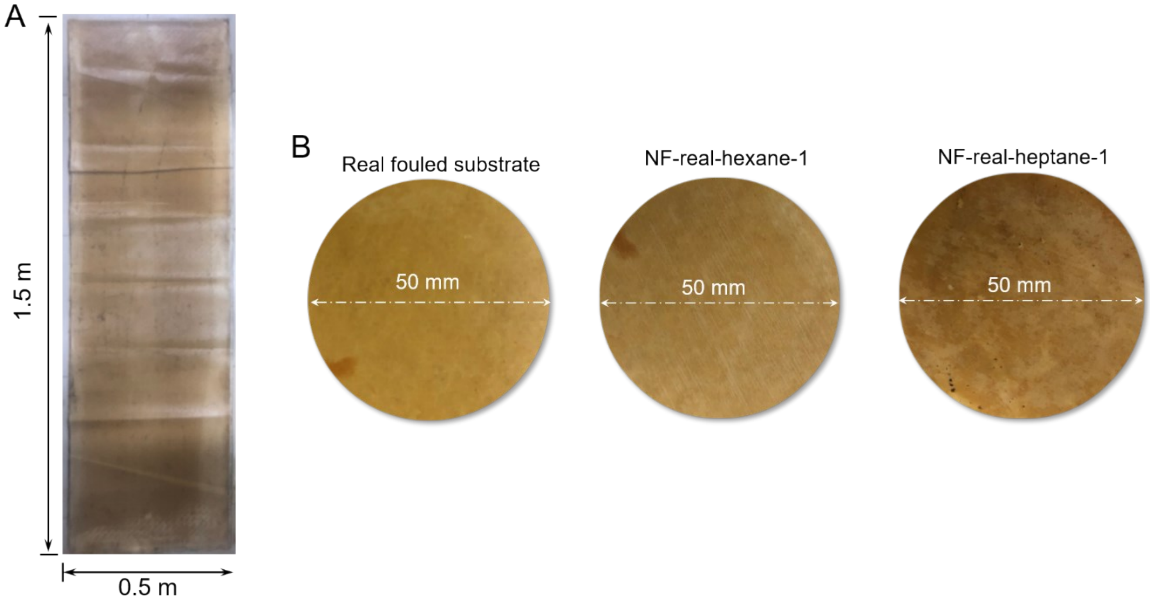

Figure S19. (A) Photo of the real fouled MF membrane element used for interfacial polymerization; (B) Photo of the real fouled MF membrane coupons. Photo credit: Ruobin Dai.

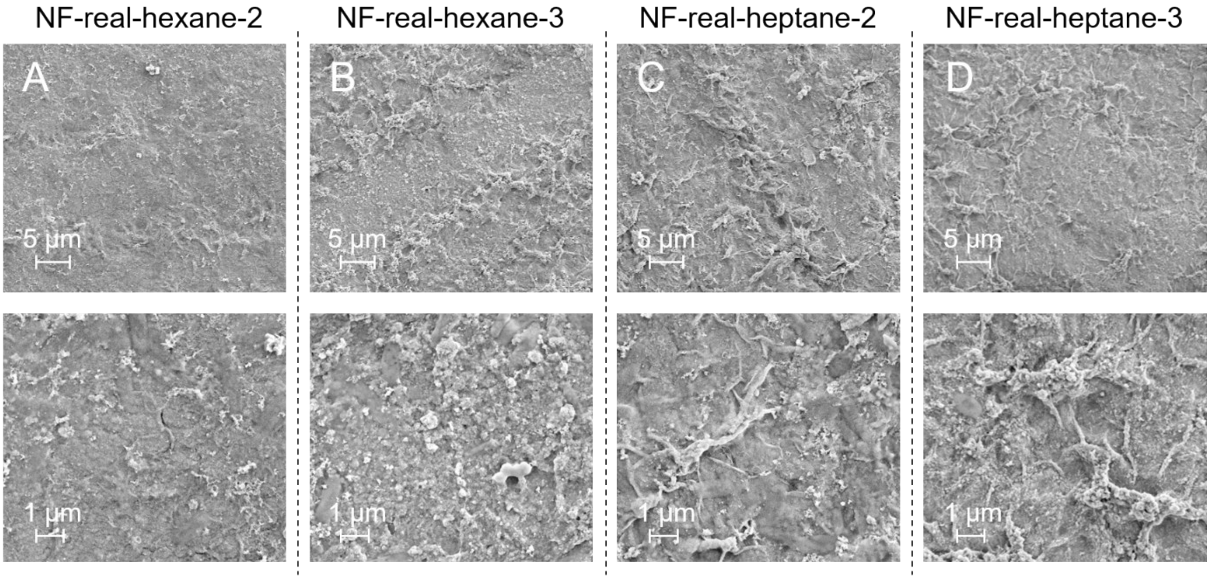

Figure S20. SEM characterizations on various TFC PA membranes upcycled from real fouled MF substrates: (A) NF-real-hexane-2; (B) NF-real-hexane-3; (C) NF-real-heptane-2; (D) NF-real-heptane-3.

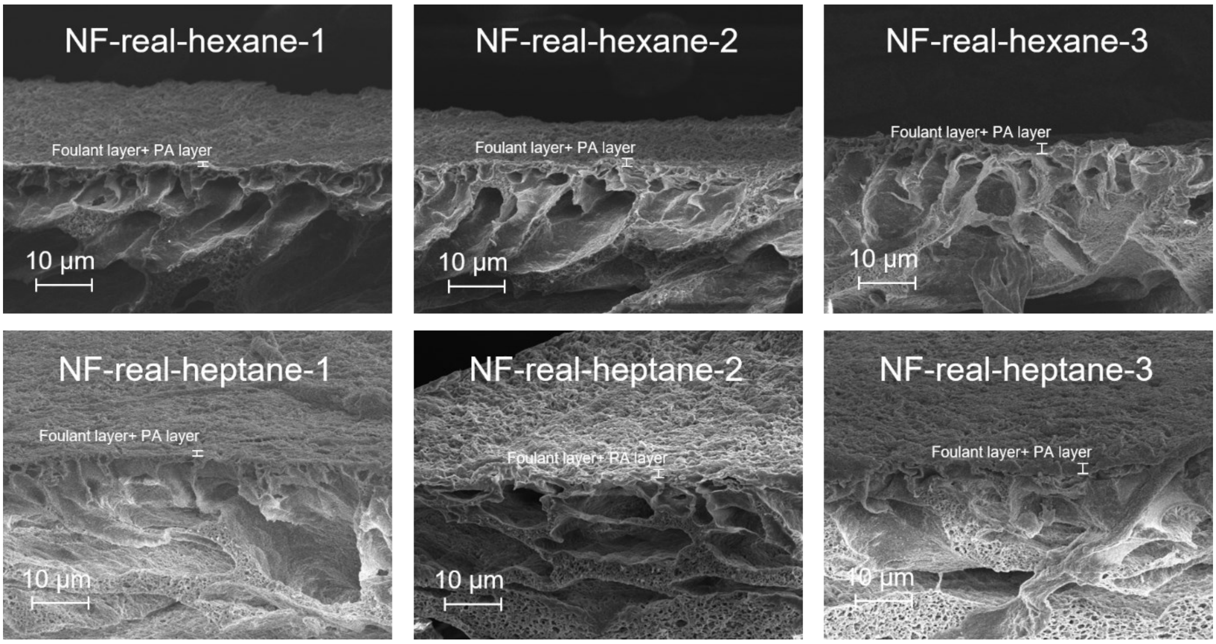

Figure S21. Cross-sectional SEM images of various TFC PA membranes upcycled from real fouled MF substrates.

Table S1. Summary of abbreviations of substrates and TFC PA membranes used in this study

Substrates	Abbreviations	TFC PA membranes	Abbreviations
PES membrane	Control	Upcycled from Control	NFcontrol
SA fouled PES membrane	SA-F	Upcycled from SA-F	NF-SA
BSA fouled PES membrane	BSA-F	Upcycled from BSA-F	NF-BSA
HA fouled PES membrane	HA-F	Upcycled from HA-F	NF-HA
EPS fouled PES membrane	EPS-F	Upcycled from EPS-F	NF-EPS

Table S2. Elemental composition of PA film of the fabricated membranes analyzed using XPS.

Membranes	**C %**	**O %**	**N %**	**O/N ratio**
NFcontrol	75.18	16.05	8.77	1.83
NF-SA	74.05	15.19	10.76	1.41
NF-BSA	73.79	15.81	10.40	1.52
NF-HA	74.30	15.94	9.76	1.63
NF-EPS	73.82	16.38	9.80	1.67

References

(1) Majorek, K. A.; Porebski, P. J.; Dayal, A.; Zimmerman, M. D.; Jablonska, K.; Stewart, A. J.; Chruszcz, M.; Minor, W. Structural and Immunologic Characterization of Bovine, Horse, and Rabbit Serum Albumins. *Molecular Immunology* **2012**, *52* (3), 174–182. https://doi.org/10.1016/j.molimm.2012.05.011.

(2) de Melo, B. A. G.; Motta, F. L.; Santana, M. H. A. Humic Acids: Structural Properties and Multiple Functionalities for Novel Technological Developments. *Materials Science and Engineering: C* **2016**, *62*, 967–974. https://doi.org/10.1016/j.msec.2015.12.001.

(3) Stevenson, F. J. *Humus Chemistry: Genesis, Composition, Reactions*, 2nd ed.; Wiley: New York, 1994.

(4) Guan, Y.-F.; Huang, B.-C.; Qian, C.; Wang, L.-F.; Yu, H.-Q. Improved PVDF Membrane Performance by Doping Extracellular Polymeric Substances of Activated Sludge. *Water Research* **2017**, *113*, 89–96. https://doi.org/10.1016/j.watres.2017.01.057.

(5) Frølund, B.; Palmgren, R.; Keiding, K.; Nielsen, P. H. Extraction of Extracellular Polymers from Activated Sludge Using a Cation Exchange Resin. *Water Research* **1996**, *30* (8), 1749–1758. https://doi.org/10.1016/0043-1354(95)00323-1.

(6) Xiao, K.; Liang, S.; Wang, X.; Chen, C.; Huang, X. Current State and Challenges of Full-Scale Membrane Bioreactor Applications: A Critical Review. *Bioresource Technology* **2019**, *271*, 473–481. https://doi.org/10.1016/j.biortech.2018.09.061.

(7) Freger, V. Swelling and Morphology of the Skin Layer of Polyamide Composite Membranes: An Atomic Force Microscopy Study. *Environ. Sci. Technol.* **2004**, *38* (11), 3168–3175. https://doi.org/10.1021/es034815u.

(8) Tan, Z.; Chen, S.; Peng, X.; Zhang, L.; Gao, C. Polyamide Membranes with Nanoscale Turing Structures for Water Purification. *Science* **2018**, *360* (6388), 518–521. https://doi.org/10.1126/science.aar6308.

(9) Pacheco, F. A.; Pinnau, I.; Reinhard, M.; Leckie, J. O. Characterization of Isolated Polyamide Thin Films of RO and NF Membranes Using Novel TEM Techniques. *Journal of Membrane Science* **2010**, *358* (1–2), 51–59. https://doi.org/10.1016/j.memsci.2010.04.032.